Comparative Thermal Degradation Studies on Glycolide/Trimethylene Carbonate and Lactide/Trimethylene Carbonate Copolymers

L. Franco, S. Bedorin, J. Puiggalí

Departament d'Enginyeria Química, Universitat Politècnica de Catalunya, Diagonal 647, Barcelona, Spain

Received 12 August 2006; accepted 13 October 2006
DOI 10.1002/app.25669
Published online in Wiley InterScience (www.interscience.wiley.com).

ABSTRACT: Thermal degradation of the glycolide/trimethylene carbonate copolymer used for bioabsorbable surgical sutures (Maxon^{TM}) has been studied by isothermal and nonisothermal methods. Thermal decomposition always follows a single mechanism, although some differences have been found between the two performed analyses. Degradation of the sample has also been compared in both an inert (N_2) and an oxidative (air) atmosphere. In all cases, the activation energy is close to 115–119 kJ/mol. A lactide/trimethylene carbonate copolymer (PLAC/PTMC) with a similar molar content of trimethylene carbonyl units to that of the indicated suture has been synthesized and characterized. Differences in the monomer reactivities have allowed to obtain a copolymer with blocky distribution of lactidyl units. Thermal decomposition of PLAC/PTMC takes place in two steps, the first one corresponding to a preferential loss of lactidyl units. Nonisothermal isoconversional methods were used to obtain the kinetic parameters of each degradation step. The complete kinetic triplets of the two studied copolymers have been determined by the Coats–Redfern and the invariant kinetic parameters (IKP) methodologies and the results were compared. © 2007 Wiley Periodicals, Inc. J Appl Polym Sci 104: 3539–3553, 2007

Key words: thermal degradation kinetics; thermal stability; thermogravimetry; glycolide; lactide; trimethylene carbonate

INTRODUCTION

The development of materials useful for biomedical applications such as bioabsorbable surgical sutures is great scientific and applied interest. An optimal suture should be easy to handle and have high tensile strength and knot security. Furthermore, any tissue reaction should be minimal, and the material should resist infection and have good elasticity and plasticity to accommodate wound swelling. Low cost is also an important consideration. Although some of the newer materials available have many of these properties, no one material is ideal, and therefore compromises must be made.[1,2]

The only natural absorbable suture available is surgical catgut. Synthetic bioabsorbable sutures can be classified into multifilamentous materials, which include, for example, polyglycolide[3] (Dexon; Sherwood-Davis and Geck) and polyglactin 910[4] (Vicryl; Ethicon), and monofilamentous forms, which include polydioxanone[5] (PDS; Ethicon), polytrimethylene carbonate copolymers[6] (Maxon; Sherwood-Davis and Geck), and polyglecaprone[7] (Monocryl; Ethicon). Monofilament sutures have the advantage of producing less tissue drag when they are pulled through the tissue. Furthermore, the smooth nature of a monofilament suture theoretically reduces the chance of wicking bacteria into the wound.[2]

MAXON, which was introduced in 1985, is prepared by a ring-opening copolymerization of glycolide and trimethylene carbonate with a 0.675 : 0.325 weight ratio.[8] The synthesis takes place in two steps where a soft segment constituted by a random distribution of the two indicated monomers is first produced, and then hard segments basically composed of glycolide units are incorporated. This suture is sterile, inert, noncollagenous, and nonantigenic. It also has a high initial tensile strength and has greater knot security than that of polydioxanone, polyglactin, or polyglycolide. Furthermore, Maxon is completely hydrolyzed in 180–210 days and is easy to handle.

Properties of sutures like degradability, crystallinity, and microstructure are receiving great attention nowadays. This interest is also focused on trimethylene carbonate copolymers with lactide[9] or glycolide.[10–13] Transesterification reactions that affect microstructure and crystallinity have been demonstrated for glycolide copolymers to occur at high temperatures.[14] However, and surprisingly, studies on the thermal degradation of useful materials as bioabsorbable sutures are relatively scarce, despite the importance of knowing the thermal stability to deter-

Correspondence to: J. Puiggalí (jordi.puiggali@upc.es).
Contract grant sponsors: CICYT and FEDER; contract grant number: MAT2003-01004.

mine processing and application conditions. In general, this kind of studies deals with homopolymers like polyglycolide,[15] polylactide,[16,17] and polydioxanone.[18,19]

The purpose of this work is to determine the thermal decomposition kinetics of the commercial glycolide/trimethylene carbonate copolymer (PGL/PTMC) in both an inert and an oxidative atmosphere. Furthermore, the thermal stability of this sample will be compared with that of a new copolymer, where glycolide units are replaced by lactide units, while the molar trimethylene carbonate ratio content remains constant.

EXPERIMENTAL

Materials

L-Lactide (Sigma-Aldrich) and trimethylene carbonate (1,3-dioxane-2-one) (Boehringer) were recrystallized from ethyl acetate, dried in a vacuum oven at room temperature, and stored over $CaCl_2$. The tin octoate catalyst was obtained from Sigma-Aldrich and used as received with no further purification. Commercially available sutures of Maxon® were purchased from Tyco Healthcare.

Copolymerization of lactide and trimethylene carbonate

Copolymers with a 0.70 : 0.30 molar ratio of lactide (LAC) and trimethylene carbonate (TMC) were synthesized by bulk ring-opening polymerization. $Sn(Oct)_2$ (0.05*M* solution in dry chloroform) was used as a catalyst, and the monomer/catalyst ratio was 5000. The monomers and initiator were mixed in a glass tube having silanized glass walls, and equipped with a magnetic stirrer and gas inlet and outlet tubes. Chloroform solvent was removed under vacuum. Polymerizations were performed under a nitrogen atmosphere at temperatures ranging from 115 to 180°C for predetermined periods of time. The obtained polymers, named with the acronym PLAC/PTMC, were directly used for NMR analysis or precipitated from chloroform solutions with methyl alcohol to remove unreacted monomers for both thermal analysis and degradation studies.

Measurements

Infrared absorption spectra were recorded with a Jasco FT/IR-4100 spectrometer in the 4000–500 cm^{-1} range from films obtained by evaporation of hexafluoroisopropanol solutions. NMR spectra were obtained with a Bruker AMX-300 spectrometer operating at 300.1 and 75.5 MHz for ^{1}H and ^{13}C-NMR investigations, respectively. Chemical displacements were calibrated using tetramethylsilane as an internal standard. Either dried dimethyl sulfoxide-d_6 (DMSO) or deuterated chloroform was used as solvents.

The molecular weights of the polymers were determined by size-exclusion chromatography (SEC) using a liquid chromatograph (Shimadzu, model LC-8A) and processed with an Empower computer program (Waters Chromatography). The average molecular weights were calculated using poly(methyl methacrylate) standards. A PL HFIP gel column (Polymer Lab) and a refractive index detector (Shimadzu RID-10A) were used. The polymers were dissolved and eluted in hexafluoroisopropanol containing CF_3COONa (0.05*M*) at the flow rate of 0.5 mL/min (injected volume 100 μL, sample concentration 1.5 mg/mL).

Basic calorimetric data were obtained via differential scanning calorimetry with a Thermal Analysis Q100 instrument using indium metal for calibration and under a flow of dry nitrogen. Thermal characterization was carried out following a protocol that involves a first heating run of the sample directly obtained from polymerization, a cooling run from the melt state, and a second heating run of the melt crystallized sample. Heating and cooling runs were performed at 20°C/min and −10°C/min, respectively.

Thermogravimetric analyses (TGA) were performed at heating rates ranging from 1 to 40°C/min for dynamic experiments with a Perkin–Elmer TGA-6 thermobalance under a flow of dry nitrogen or of air. The sizes of TGA samples ranged from 10 to 15 mg. Isothermal analyses were carried at temperatures ranging from 250 to 290°C in an oxidative atmosphere.

Deconvolution of the derivative thermogravimetric curve was performed with the Peak.fit program by Jandel Scientific Software using a mathematical function known as ''asymmetric double sigmoidal.''

Isothermal analyses

In an isothermal degradation test, the experimental data must fit the standard kinetic equation:

$$d\alpha/dt = k(T)f(\alpha) \quad (1)$$

where $k(T)$ is the kinetic rate constant, t is time, α is the normalized degree of degradation or conversion, and $f(\alpha)$ is the differential conversion function.

The conversion is calculated in terms of mass loss as

$$\alpha = \frac{W_0 - W}{W_0 - W_\infty} \quad (2)$$

where W_0, W, and W_∞ are, respectively, the initial polymer weight, the actual weight at each point of the

TABLE I
Algebraic Expressions of $f(\alpha)$ and $g(\alpha)$ for the Kinetics Models Considered in This Work

Symbol	Reaction model	$f(\alpha)$	$g(\alpha)$
$A_{3/2}$	Avrami–Erofeev equation ($n = 1.5$)	$3/2\ (1-\alpha)\ [-\ln(1-\alpha)]^{1/3}$	$[-\ln(1-\alpha)]^{2/3}$
A_2	Avrami–Erofeev equation ($n = 2$)	$2\ (1-\alpha)\ [-\ln(1-\alpha)]^{1/2}$	$[-\ln(1-\alpha)]^{1/2}$
A_3	Avrami–Erofeev equation ($n = 3$)	$3\ (1-\alpha)\ [-\ln(1-\alpha)]^{2/3}$	$[-\ln(1-\alpha)]^{1/3}$
A_4	Avrami–Erofeev equation ($n = 4$)	$4\ (1-\alpha)\ [-\ln(1-\alpha)]^{3/4}$	$[-\ln(1-\alpha)]^{1/4}$
D_1	One-dimensional diffusion or parabolic law	$(2\alpha)^{-1}$	α^2
D_2	Two-dimensional diffusion (Valensi equation)	$[-\ln(1-\alpha)]^{-1}$	$(1-\alpha)\ln(1-\alpha)+\alpha$
D_3	Three-dimensional diffusion (Jander equation)	$3/2(1-\alpha)^{2/3}\ [1-(1-\alpha)^{1/3}]^{-1}$	$[1-(1-\alpha)^{1/3}]^2$
D_4	Three-dimensional diffusion (Ginstling–Brounshtein equation)	$3/2(1-\alpha)^{1/3}\ [1-(1-\alpha)^{1/3}]^{-1}$	$1-2/3\alpha-(1-\alpha)^{2/3}$
R_2	Contracting area (cylindrical symmetry)	$2(1-\alpha)^{1/2}$	$1-(1-\alpha)^{1/2}$
R_3	Contracting volume (spherical symmetry)	$3(1-\alpha)^{2/3}$	$1-(1-\alpha)^{1/3}$
$n+m=2;\ n=1.5$	Autocatalytic reaction	$(\alpha)^{0.5}(1-\alpha)^{1.5}$	$[(1-\alpha)\alpha^{-1}]^{-0.5}(0.5)^{-1}$
$n+m=2;\ n=1.9$	Autocatalytic reaction	$(\alpha)^{0.1}(1-\alpha)^{1.9}$	$[(1-\alpha)\alpha^{-1}]^{-0.9}(0.9)^{-1}$
$n=2$	Second-order	$(1-\alpha)^2$	$-1+(1-\alpha)^{-1}$
$n=3$	Third-order	$(1-\alpha)^3$	$2^{-1}[-1+(1-\alpha)^{-2}]$
F_1 or $n=1$	Random nucleation or first-order kinetics	$(1-\alpha)$	$-\ln(1-\alpha)$
Power	Power law	$2(\alpha)^{1/2}$	$(\alpha)^{1/2}$

degradation curve, and the final weight at the end of the degradation process.

The temperature dependence of the kinetic rate constant is assumed to follow an Arrhenius form:

$$k = A\exp(-E/RT) \tag{3}$$

where T is the absolute temperature, R is the gas constant, and A and E are the preexponential and the activation energy for the decomposition reaction, respectively.

The major disadvantage of this approach is that complete degradation may require significant amounts of time (in the present case, from 2 to 10 h). However, the simplicity of analysis and the fact that no approximations are needed must be pointed out. For predictive purposes, it is possible to create an isothermal master curve by simply scaling the raw data with time. This is accomplished by dividing the time on the abscissa axis by the time required for a conversion of 0.5 ($t_{1/2}$). In this way, degradation curves obtained at different temperatures collapse onto a single one.

Dynamic methods

According to the nonisothermal kinetic theory, thermal degradation of a polymer can be expressed by the following function:

$$\frac{d\alpha}{dT} = \frac{1}{\beta}A\exp\left(-\frac{E}{RT}\right)f(\alpha) \tag{4}$$

where β is the heating rate and the other terms have the above indicated meaning.

The integration of $f(\alpha)$ leads to:

$$g(\alpha) = \int_0^\alpha \frac{d\alpha}{f(\alpha)} \tag{5}$$

The differential ($f(\alpha)$) and the integral ($g(\alpha)$) conversion functions may take different forms according to the solid state reaction mechanism.[20] These are summarized in Table I.

The most probable mechanism can be determined by using the Coats–Redfern approximation[21] to solve eq. (5) and considering that $2RT/E \ll 1$, this equation may be rewritten as:

$$\ln\frac{g(\alpha)}{T^2} = \ln\left(\frac{AR}{\beta E}\right) - \frac{E}{RT} \tag{6}$$

For a given kinetic model, the linear representation of $\ln[g(\alpha)/T^2]$ versus $1/T$ makes it possible to determine E and A from the slope and the ordinate at the origin, respectively. The model can be selected taking into account the linear regression coefficient (r) and the agreement of the activation energy with that estimated by isoconversional methods such as the Kissinger–Akahira–Sunose (KAS),[22] Friedman,[23] Kissinger[22] and Flynn–Wall–Ozawa (FWO) methods.[24,25]

The KAS method is based on eq. (7), which is obtained by reordering the above-indicated equation of the integral conversion function:

$$\ln\frac{\beta}{T^2} = \ln\left[\frac{AR}{g(\alpha)E}\right] - \frac{E}{RT} \tag{7}$$

For each degree of conversion the activation energy can be obtained from the slope of linear representation of $\ln(\beta/T^2)$ versus $1/T$.

The Friedman method is based on eq. (8), which in this case derives from the logarithmic form of the rate eq. (4):

$$\ln\left(\beta\frac{d\alpha}{dT}\right) = \ln A + \ln f(\alpha) - \frac{E}{RT} \tag{8}$$

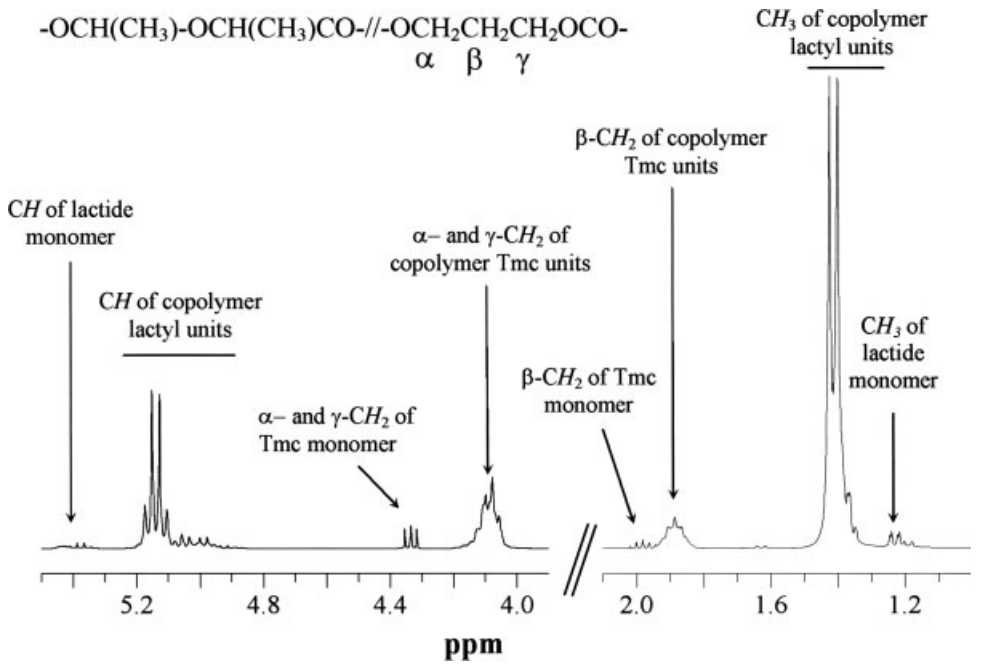

Figure 1 ^{1}H-NMR spectrum in DMSO of PLAC/PTMC obtained at 150°C for 28 h with $Sn(Oct)_2$ as a catalyst. The arrows indicate the characteristic signals of the monomers.

For each degree of conversion, the plot of ln ($\beta\, d\alpha/dT$) versus $1/T$, obtained from thermograms recorded at several heating rates, should be a straight line whose slope allows the evaluation of the activation energy.

The Kissinger equation can be considered a particular case of eq. (7) applied for $\alpha = \alpha_{max}$ (the conversion at the maximum weight loss rate) and assuming $f(\alpha) = (1 - \alpha)^n$:

$$\ln\frac{\beta}{T_{max}^2} = \ln\frac{AR}{E} + \ln\left[n(1-\alpha_{max})^{n-1}\right] - \frac{E}{RT_{max}} \quad (9)$$

where T_{max} is the temperature at the inflection point of the thermodegradation curves, which corresponds to the maximum reaction rate. In this case, the activation energy can be determined from the slope of the linear plot of $\ln(\beta/T_{max}^2)$ versus $1/T_{max}$. It is now well-known that this method may also be applied when $f(\alpha)$ correspond to other kinetic models.[26]

The Flynn–Wall–Ozawa eq. (10) is one of the integral methods by which the activation energy can be determined without knowing the reaction order:[24,25]

$$\ln\beta = \ln\frac{0.0048AE}{g(\alpha)R} - 1.0516\frac{E}{RT} \quad (10)$$

The activation energy can be calculated for different conversions from the slopes of the linear plots of ln β versus $1/T$.

Another method used to evaluate the kinetic parameters is the IKP (invariant kinetic parameters) method.[27,28] According to this procedure, the values of the activation parameters, obtained from various forms of $f(\alpha)$, are correlated through an apparent compensation effect:

$$\ln A = \alpha^* + \beta^* E \quad (11)$$

where α* and β* are constants (the compensation effect parameters).

To apply this method, the values of ln A_i versus E_i at each heating rate (β_i) were plotted. These

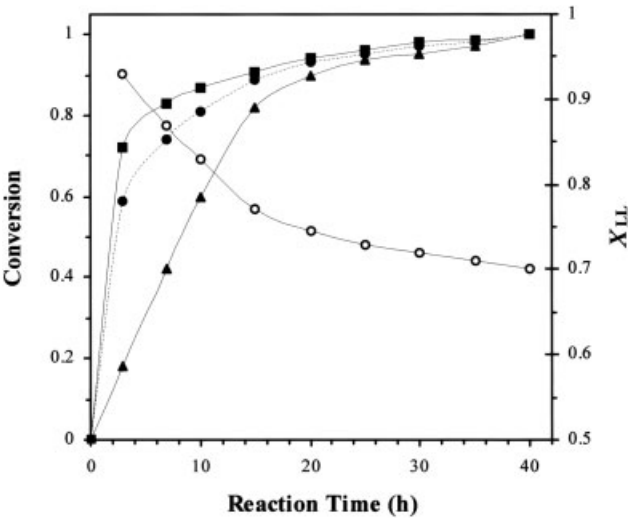

Figure 2 Molar percentage of lactide units in PLAC/PTMC samples (○), and lactide (■), trimethylene carbonate (▲), and total conversions versus polymerization time (●). Polymerizations were performed at 115°C using $Sn(Oct)_2$ as a catalyst.

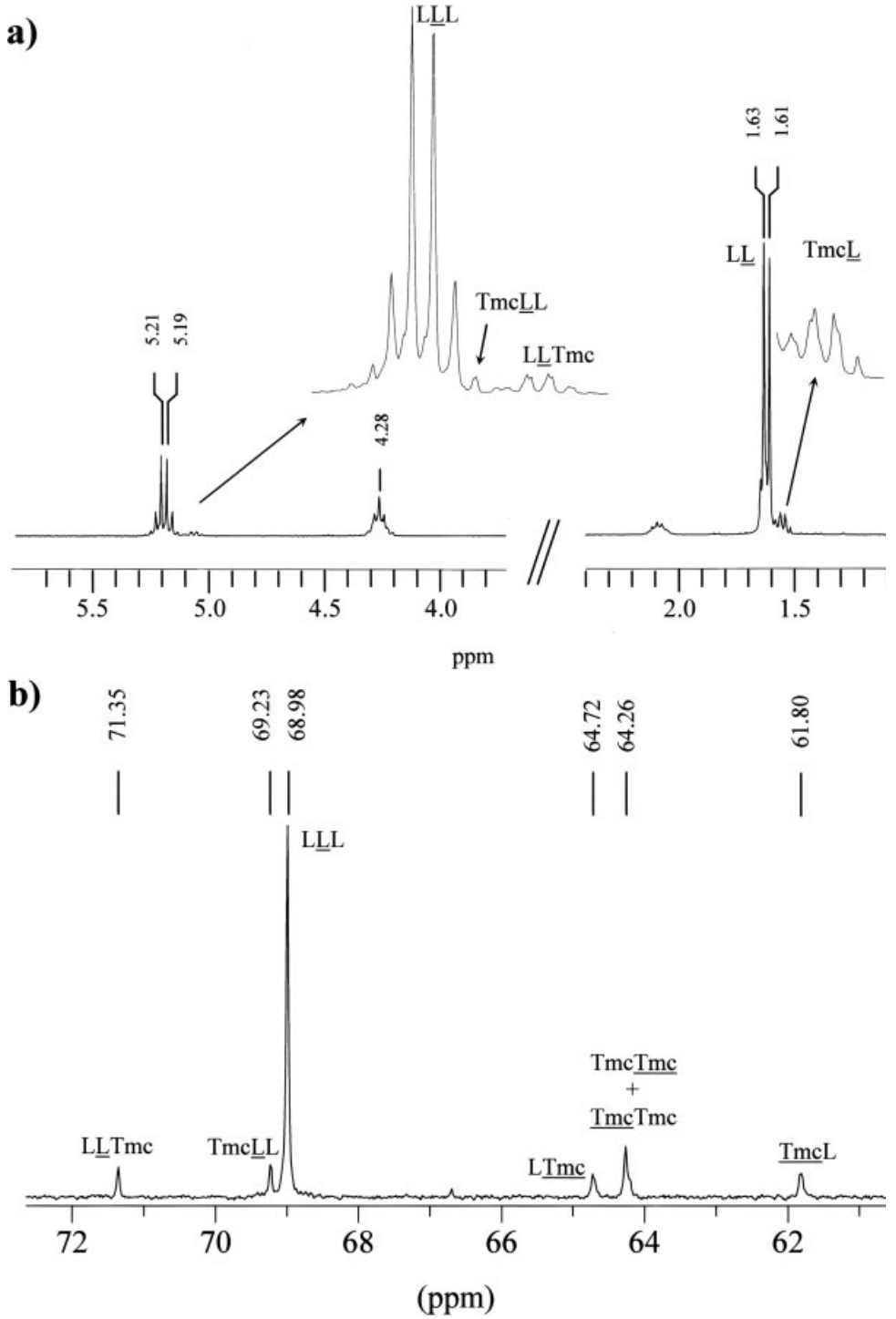

Figure 3 ^{1}H-NMR (a) and ^{13}C-NMR (b) spectra in $CDCl_3$ of a PLAC/PTMC sample prepared at 150°C for 40 h and using $Sn(Oct)_2$ as a catalyst. A magnification of the ^{1}H-NMR spectra signals corresponding to some lactyl protons (5.30–5.01 and 1.57–1.50 ppm) is shown in the inset. Only signals corresponding to the CH and $OCH_2CH_2CH_2OCO$ carbons are shown in the ^{13}C-NMR spectra (72–61 ppm).

parameters were obtained using the Coats–Redfern methodology for the different kinetic models studied (Table I). The plot allowed the α_i^* and β_i^* constants to be determined from the intersection at the origin and the slope, respectively. Furthermore, the straight lines ln A_i versus E_i for each heating rate should intersect at a point, which corresponds to the true values of A and E. These are called the invariant activation parameters (A_{inv}, E_{inv}). Certain variations of the experimental conditions actually determine a region of intersection in the ln A, E space. For this reason, the evaluation of the invari-

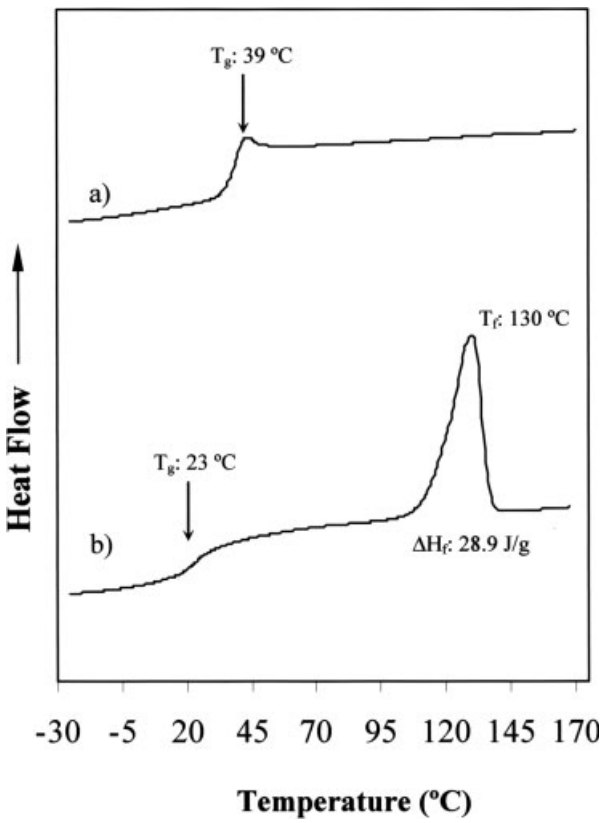

Figure 4 Calorimetric DSC scans performed with a PLAC/PTMC sample synthesized at 150°C for 40 h and using $Sn(Oct)_2$ as a catalyst. (a) Second heating run performed with a sample previously cooled (−10°C/min) from the melt state, (b) First heating run of a sample coming directly from synthesis.

ant activation parameters is performed using the following relation:

$$\ln A_{\text{inv}} = \alpha_i^* + \beta_i^* E_{\text{inv}} \tag{12}$$

Thus, a plot of α_i^* versus β_i^* is actually a straight line whose parameters allow evaluation of the invariant activation parameters.

RESULTS AND DISCUSSION

Synthesis of the PLAC/PTMC copolymer

^{1}H-NMR spectra taken at low conversions (Fig. 1) clearly show the signals of unreacted lactide (5.37 and 1.22 ppm) and trimethylene carbonate (4.35 and 1.98 ppm) monomers, which can be well distinguished from those corresponding to the units incorporated into the polymer chain (5.20–4.90 and 1.47–1.33 ppm for lactyl groups (L); 4.15–4.03 ppm for the α- and γ-methylene protons and 1.93–1.82 ppm for the β-methylene protons of trimethylene carbonate groups (Tmc)). The respective areas were used to determine the lactide (C_{LL}) and trimethylene carbonate (C_{Tmc}) conversions, the total conversion of the reaction (C), and the lactidyl (X_{LL}) molar content of copolymers according to the following equations:

$$X_{\text{LL}} = S_{5.20-4.90}/(S_{5.20-4.90} + 0.5S_{4.15-4.03}) \tag{13}$$

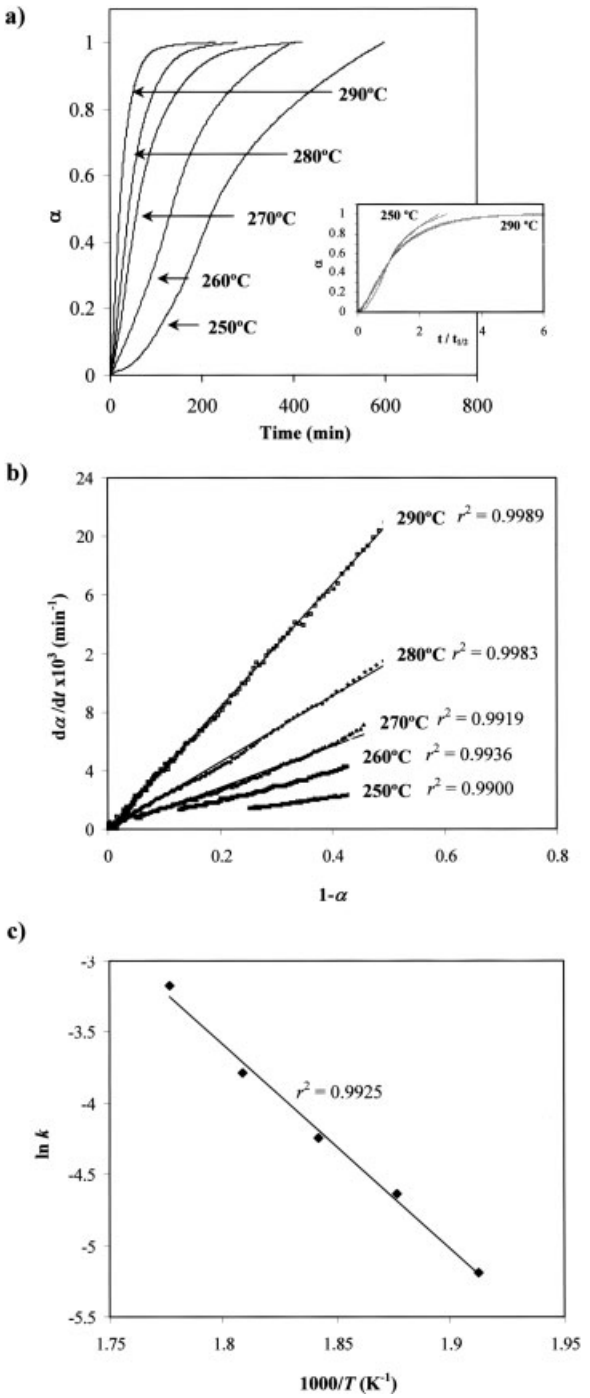

Figure 5 Isothermal analysis for the decomposition of the PGL/PTMC (Maxon) under air: (a) Plot of the degree of conversion (α) versus time at different isothermal temperatures. The inset shows the corresponding kinetic master curve, (b) Plot of the degree of conversion $d\alpha/dt$ versus (1 – α) at different isothermal temperatures, (c) Arrhenius plot.

TABLE II
Thermogravimetric Data of PGL/PTMC (Maxon) Samples

Atmosphere	β (°C/min)	$T_{20\%}$ (°C)	$T_{50\%}$ (°C)	$T_{70\%}$ (°C)	$T_{90\%}$ (°C)	T_{max} (°C)
N_2	3	311.57	327.24	334.17	344.19	331.52
	5	317.69	333.78	341.85	352.42	336.59
	10	333.25	352.48	361.86	373.72	361.36
	20	352.25	371.63	380.46	391.48	378.31
	30	369.39	388.03	395.67	406.19	391.04
Air	3	307.34	324.29	332.21	344.39	328.94
	5	322.75	339.66	346.97	358.13	343.97
	10	339.53	356.42	364.35	375.55	360.52
	20	355.98	374.49	382.82	394.86	379.34
	30	369.51	386.79	395.30	407.84	389.47

$$C_{LL} = S_{5.20-4.90}/(S_{5.20-4.90} + S_{5.37}) \quad (14)$$

$$C_{Tmc} = S_{4.15-4.03}/(S_{4.15-4.03} + S_{4.35}) \quad (15)$$

$$C = 1/[(X_{LL}/C_{LL}) + ((1 - X_{LL})/(C_{Tmc})] \quad (16)$$

where S means the area of the corresponding NMR signals.

Sublimation of monomers was negligible since the calculated composition of polymers attained at a high reaction conversion was in agreement with the comonomer feed ratio.

Copolymerizations were investigated at different reaction times (Fig. 2) and temperatures.

The results obtained with constant monomer composition and catalyst ratio showed that lactide was preferentially polymerized and that trimethylene carbonate was incorporated later. Thus, lactide conversion was almost quantitative in copolymerizations carried out at 115°C for 96 h, whereas a complete Tmc conversion was only reached after more than 144 h at the indicated temperature. These reactivity differences favor a blocky microstructure where polylactide segments are preferentially formed at the initial and polymerization stages. Higher reaction temperature results in lower differences in reactivity and less time required to reach a total conversion (for example only 20 h at 180°C and 35 h at 150°C). A temperature of 150°C was selected to prepare the PLAC/PTMC sample used in the TGA since the polymerization time was reasonable and lactide reactivity appeared sufficiently greater than comonomer reactivity to ensure a preferential blocky distribution of this monomer by using this single step synthesis. This distribution tries to mimic the hard polyglycolide segments characteristic of commercial Maxon samples.

Furthermore, GPC measures indicated that the molecular weight of the polymer was maximum at around this temperature. Weight average molecular weights of 15,000, 20,000, and 18,000, and polydispersity indices of 2.1, 1.6, and 1.5 were measured for the samples synthesized at 115, 150, and 180°C, respectively. High reaction temperatures seem to favor a decomposition that renders the initial lactide monomer again since ring-opening polymerization is, in fact, an equilibrium reaction and causes a slight decrease in the molecular weight of the sample. This is confirmed by the small lactide signals that can be observed in the NMR spectra of the polymerization medium when the reaction is conducted at a high temperature and long reaction time. In this case, the calculated lactide conversion slightly decreases from 100%, whereas the trimethylene carbonate conversion reaches the maximum value.

^{1}H- and ^{13}C-NMR spectra can be used to investigate the copolymer microstructure since some triads and dyads can be well differentiated in the spectra registered in deuterated chloroform solutions, as previously reported.[29] The sequences are named indicating their constitutive units by using the abbreviations L and Tmc as the lactyl and trimethylene carbonate residues, respectively.

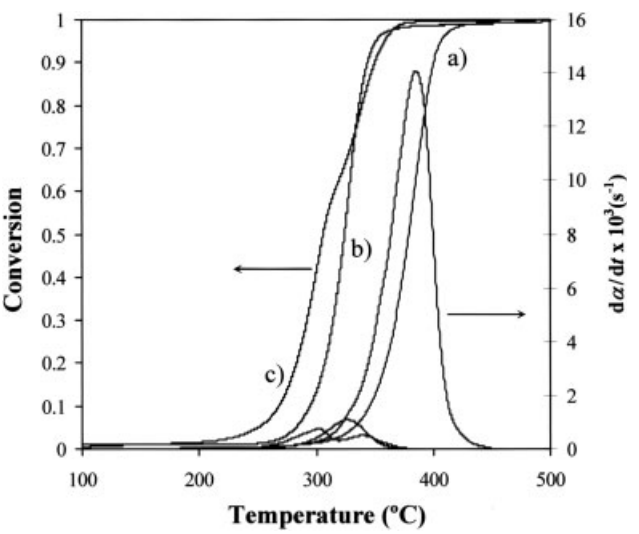

Figure 6 Degree of conversion (α) and derivative curve ($d\alpha/dt$) versus temperature for the decomposition under air of: (a) PGL/PTMC (Maxon) at a heating rate of 40°C/min, (b) PLAC/PTMC at a heating rate of 40°C/min, and (c) PLAC/PTMC at a heating rate of 3°C/min.

The proton spectrum showed an intense quadruplet at around 5.20 ppm, which is attributed to the CH group of the L*L*L triad [Fig. 3(a)]. In the same way, a low intensity quadruplet corresponding to the L*L*Tmc triad was observed at around 5.05 ppm, as well as the upfield peak of the quadruplet corresponding to the Tmc*L*L triad. It is remarkable that no a Tmc*L*Tmc sequence, which should be expected at around 4.99 ppm, was detected. This triad is a consequence of a transesterification reaction that occurs inside the lactidyl units, and consequently must only appear when polymerizations are conducted at very high temperatures and for long reaction times. Doublets corresponding to the L*L* and Tmc*L* sequences could also be detected at around 1.62 and 1.55 ppm, respectively, in agreement with the reported dyad sensitivity of the CH_3 protons. In summary, the proton spectrum clearly indicated that lactide units have a preferential blocky distribution, as could be expected from both their higher reactivity and higher molar content in the reaction medium. Protons of the trimethylene carbonate units appeared as multiplet signals that are not sufficiently split for the different dyads to be distinguished.

Average block lengths were achieved by considering the 72–61 ppm zone of the ^{13}C-NMR spectra, where signals attributed to the CH group of lactyl units and the α and γ methylene groups of trimethylene carbonate residues appear [Fig. 3(b)]. Thus, L*L*L, Tmc*L*L, and L*L*Tmc triplets can be well distinguished at 68.98, 69.23, and 71.35 ppm, respectively, the corresponding relative areas being close to 15, 1, and 1. At this point, no Tmc*L*Tmc triplet, indicative of transesterification reactions, was observed either since its chemical shift is expected at around 71.66 ppm.[29]

An average block length for the lactyl units (L_L^e) of 17 could be estimated from the concentration of the indicated triads:

$$L_L^e = 1 + (([\mathrm{LLL}] + [\mathrm{TmcLL}])/([\mathrm{LLTmc}] + [\mathrm{TmcLTmc}])) = 1 + (([\mathrm{LLL}] + [\mathrm{LLTmc}]) + [\mathrm{LLTmc}])/([\mathrm{TmcLL}] + [\mathrm{TmcLTmc}]) \quad (17)$$

The α-methylene carbon of Tmc showed a dyad sensitivity (L*Tmc* and Tmc*Tmc* at 61.83 and 64.26 ppm, respectively) and so did the γ-methylene carbon (*Tmc*Tmc and *Tmc*L at 64.26 and 64.75 ppm, respectively). It should be pointed out that L*Tmc* and *Tmc*L dyads have the same relative intensity (1.28), a feature indicative of an equal proportion of the Tmc*Tmc* and *Tmc*Tmc dyads that appear overlapped at 64.26 ppm (total area of 2.72). Hence, the concentration of the four triads involving the Tmc units was estimated. A block length close to 2 was derived for the trimethylene carbonate units (L_{Tmc}^e) by applying eq. (18):

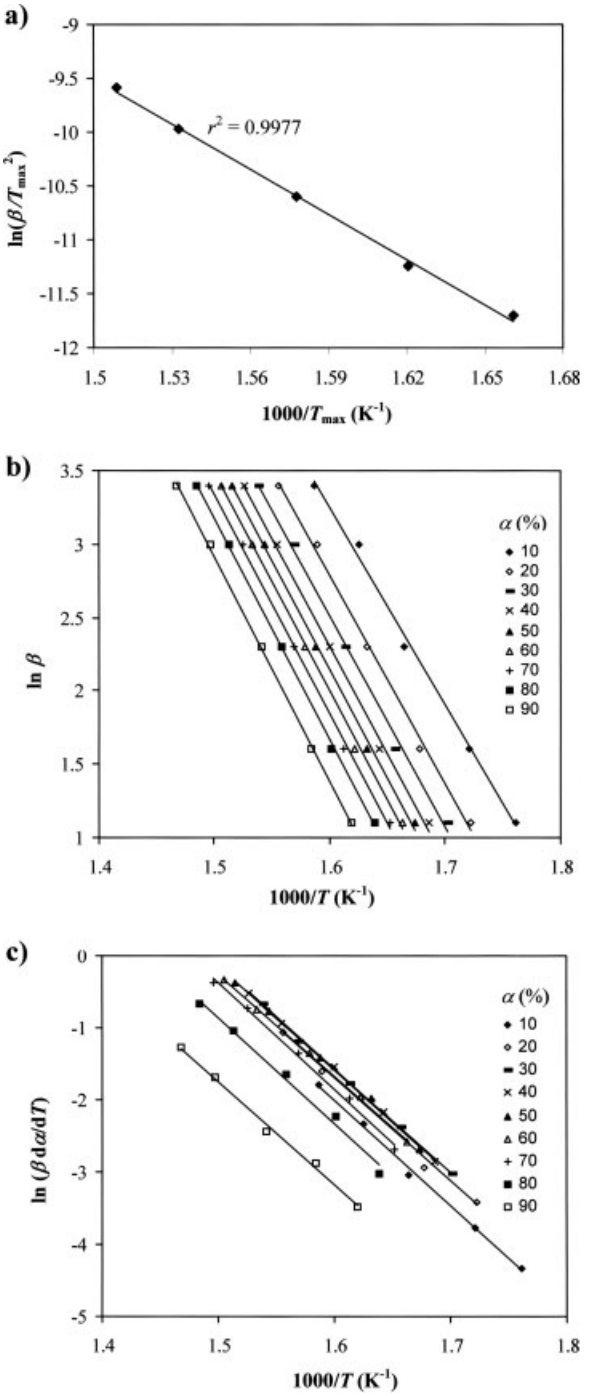

Figure 7 Kissinger (a), FWO (b), and Friedman (c) plots for the thermal decomposition of the PGL/PTMC (Maxon) sample in air.

$$L_L^e = 1 + (([\mathrm{TmcTmcTmc}] + [\mathrm{LTmcTmc}])/([\mathrm{TmcTmcL}] + [\mathrm{LTmcL}])) \quad (18)$$

The DSC heating trace of a solution precitated sample (Fig. 4) showed a single melting peak at 130°C, which was indicative of a crystalline domain rich on lactide units, as was expected from the NMR microstructural analysis. A degree of crystallinity close to 40% was

TABLE III
Activation Energies of PGL/PTMC (Maxon) in Both N_2 and in Air Atmosphere Obtained by the Flynn–Wall–Ozawa and Friedman Methods

	Flynn–Wall–Ozawa method				Friedman method			
	N_2		Air		N_2		Air	
Conversion α	E (kJ/mol)	r	E (kJ/mol)	r	E (kJ/mol)	r	E (kJ/mol)	r
0.1	113	0.98919	106	0.99800	114	0.98955	121	0.99840
0.2	116	0.98929	112	0.99825	113	0.99805	119	0.99464
0.3	116	0.98980	114	0.99850	111	0.99519	118	0.99935
0.4	116	0.99156	116	0.99880	112	0.99765	121	0.99945
0.5	116	0.99328	117	0.99910	112	0.99589	120	0.99915
0.6	117	0.99489	118	0.99935	112	0.99469	118	0.99965
0.7	118	0.99619	118	0.99945	116	0.99755	122	0.99775
0.8	119	0.99685	119	0.99970	119	0.99745	123	0.99494
0.9	121	0.99710	121	0.99970	119	0.99915	119	0.99715
Mean	117		116		114		120	

calculated taking into account the reported value[30] (93 J/g) for a 100% crystalline poly(L-lactide) (PLLA) and the experimental heat of fusion referred to the lactide weight of the PLAC/PTMC sample.

The melting point depression for a copolymer with a random distribution was calculated by applying the well-known Flory equation:[31]

$$1/T_m = 1/T_m^\circ - (R/\Delta H_m^\circ) \ln X_G \qquad (19)$$

where T_m and T_m° are the equilibrium melting temperatures of the copolymer and the PLLA homopolymer, respectively, H_m° is the equilibrium heat of fusion of the PLLA homopolymer, and R is the gas constant. An equilibrium melting temperature of 158°C was estimated assuming a lactyl molar content of 0.82 (X_{LL} : 0.70) and the reported T_m° values[32,33] (480–485 K).

PLAC/PTMC hardly crystallizes from the melt state, as deduced from the second DSC heating run (Fig. 4). The amorphous phase showed a single glass transition temperature of 30°C, which was intermediate between those of the corresponding homopolymers −16°C and 63°C for poly(TMC) and poly(L-lactide), respectively, and indicates the existence of a single phase. It should be pointed out that T_g decreases to 23°C in the solution crystallized sample, a feature suggesting the expected increase in Tmc content in the amorphous phase.

Kinetics of thermal degradation of PGL/PTMC

Figure 5(a) shows the results of isothermal TGA experiments at temperatures of 250, 260, 270, 280, and 290°C performed on commercial PGL/PTMC sutures under air. A total decomposition was achieved in reasonable times to perform this isothermal analysis. Thus, 2 and 10 h were required for the highest and lowest assayed temperatures, respectively. The isothermal master curve obtained by scaling the raw data with time was indicative of a single decomposition mechanism or the existence of multiple mechanisms with the same reaction order.

Kinetic rate constants were evaluated at the different temperatures by fitting the data to eq. (1). Linear plots were attained [Fig. 5(b)] assuming a first-order mechanism, F1 model, ($f(\alpha) = (1 - \alpha)$). The $k(T)$ values deduced from the slopes were then fitted to the Arrhenius equation [Fig. 5(c)] leading to an activation energy of 119 kJ/mol and a preexponential factor of 4.24×10^9 min^{-1} ($\ln A = 22.17$).

Isothermal thermogravimetric degradation studies performed on polyglycolide under air[15] suggested a first-order mechanism too, which was explained by an intramolecular ester interchange that renders the glycolide monomer as the major decomposition route. The relatively low value found for the preexponential factor (3.53×10^{11} min^{-1}) was taken as an indication of a fair degree of steric order in the transition state of

TABLE IV
Activation Energies (kJ/mol) of the Studied Polymers Determined by Different Isoconversional Methods

		Isoconversional method		
Polymer	Atmosphere	Kissinger	FWO	Friedman
PGL/PTMC (Maxon)	N_2	111	117	114
PGL/PTMC (Maxon)	Air	117	116	120
PLAC/PTMC Single step	Air	75	79	84
PLAC/PTMC 1st step	Air	93	110	119
PLAC/PTMC 2nd step	Air	149	139	162

TABLE V
Activation Energies of PGL/PTMC (Maxon) in N_2 Obtained by the Coats–Redfern Method

	3°C/min		5°C/min		10°C/min		20°C/min		30°C/min	
	E (kJ/mol)	*r*	*E* (kJ/mol)	*r*	*E* (kJ/mol)	*r*	*E* (kJ/mol)	*r*	*E* (kJ/mol)	*r*
Power	68	0.9951	65	0.9934	59	0.9894	63	0.9945	72	0.9966
$A_{3/2}$	115	0.9995	125	0.9989	116	0.9999	124	0.9993	138	0.9981
A_2	96	0.9983	91	0.9989	85	0.9999	90	0.9992	101	0.9980
A_3	60	0.9981	57	0.9987	53	0.9999	57	0.9992	64	0.9978
A_4	43	0.9980	40	0.9986	32	0.9998	40	0.9991	45	0.9976
F_1	201	0.9984	192	0.9989	180	0.9999	191	0.9993	213	0.9982
R_2	171	0.9990	163	0.9985	152	0.9978	162	0.9994	182	0.9996
R_3	181	0.9992	172	0.9991	160	0.9990	171	0.9999	191	0.9995
D_1	301	0.9961	288	0.9947	266	0.9919	286	0.9958	321	0.9973
D_2	342	0.9984	327	0.9976	305	0.9963	326	0.9986	364	0.9991
D_3	371	0.9993	354	0.9991	331	0.9991	353	0.9999	394	0.9995
D_4	345	0.9988	330	0.9983	307	0.9973	328	0.9992	367	0.9995
$n = 1.5$	236	0.9944	225	0.9958	212	0.9978	225	0.9953	249	0.9933
$n = 1.5$, $m = 0.5$	133	0.9869	126	0.9891	120	0.9919	126	0.9876	140	0.9848
$n = 1.9$, $m = 0.1$	248	0.9877	236	0.9897	224	0.9924	236	0.9884	261	0.9857
$n = 2$	277	0.9878	263	0.9898	250	0.9925	263	0.9885	291	0.9858
$n = 3$	369	0.9719	350	0.9748	336	0.9782	351	0.9720	386	0.9686

the rate controlling step. This feature allowed a thermal decomposition based on molecular decarboxylation or decarbonylation reactions to be discarded.

Transesterification reaction giving rise to both glycolide and trimethylene carbonate rings could also be expected in the decomposition of PGL/PTMC samples. The isothermal parameters are comparable with those reported for polyglycolide, although this polymer showed higher values for the activation energy (153 kJ/mol) and the preexponential factor.

Nonisothermal degradation studies on PGL/PTMC samples were also undertaken using both an inert and an oxidative atmosphere provided by a flow of nitrogen and air, respectively. Data of thermogravimetric curves obtained at five heating rates varying from 3 to 30°C/min are summarized in Table II, and a representative curve is plotted in Figure 6. Inspection of data reveals that degradation proceeds in a single step. Note for instance the appearance of the thermogravimetric curve obtained at the lowest heating rate shown in Figure 6. The degradation processes also seems very similar in nitrogen and air, a feature that contrasts with the differences reported for polyglycolide,[15] where the activation energy and the preexponential factor decreased to 135 kJ/mol and 1.25×10^{10} min^{-1}, respectively, when decomposition took place under N_2.

Figure 7 shows the characteristic plots corresponding to the Kissinger, Flynn–Wall–Ozawa and Friedman analyses of PGL/PTMC samples for experiments performed under air, whereas complete isoconversional data are summarized in Table III.

TABLE VI
Activation Energies of PGL/PTMC (Maxon) in Air Obtained by the Coats–Redfern Method

	3°C/min		5°C/min		10°C/min		20°C/min		30°C/min	
	E (kJ/mol)	*r*	*E* (kJ/mol)	*r*	*E* (kJ/mol)	*r*	*E* (kJ/mol)	*r*	*E* (kJ/mol)	*r*
Power	60	0.9929	64	0.9960	68	0.9933	65	0.9946	71	0.9892
$A_{3/2}$	117	0.9991	122	0.9961	133	0.9993	127	0.9984	140	0.9995
A_2	85	0.9990	89	0.9959	97	0.9993	93	0.9984	102	0.9995
A_3	53	0.9989	56	0.9955	61	0.9992	58	0.9982	64	0.9995
A_4	38	0.9988	39	0.9949	43	0.9991	41	0.9980	46	0.9994
F_1	180	0.9991	188	0.9963	205	0.9993	196	0.9985	215	0.9996
R_2	153	0.9984	160	0.9982	174	0.9988	166	0.9989	181	0.9973
R_3	161	0.9990	169	0.9980	183	0.9994	176	0.9992	192	0.9985
D_1	269	0.9945	284	0.9969	305	0.9946	293	0.9958	316	0.9914
D_2	307	0.9975	323	0.9982	347	0.9978	334	0.9982	361	0.9958
D_3	332	0.9991	348	0.9981	377	0.9995	362	0.9993	394	0.9986
D_4	309	0.9981	325	0.9983	350	0.9985	337	0.9988	365	0.9968
$n = 1.5$	211	0.9964	220	0.9912	242	0.9960	232	0.9944	256	0.9977
$n = 1.5$, $m = 0.5$	119	0.9905	123	0.9825	137	0.9892	130	0.9868	145	0.9924
$n = 1.9$, $m = 0.1$	221	0.9911	230	0.9836	254	0.9899	243	0.9876	271	0.9928
$n = 2$	247	0.9912	257	0.9837	284	0.9899	272	0.9877	302	0.9929
$n = 3$	330	0.9776	341	0.9667	381	0.9748	364	0.9716	409	0.9795

TABLE VII
Kinetic Parameters Associated with the Thermal Degradation of PGL/PTMC (Maxon) in N_2 and Air, and PLAC/PTMC in Air

Polymer	E_{inv} (kJ/mol)	ln A_{inv} (min^{-1})	k^a (min^{-1})	Model	E (kJ/mol)	ln A (min^{-1})
PGL/PTMC (N_2)	115	20.59	0.280	$A_{3/2}$	115	20.86
PGL/PTMC (air)	117	20.99	0.286	$A_{3/2}$	117	21.09
PLAC/PTMC (air) single step	77	13.96	0.507	A_2	82	15.04
PLAC/PTMC (air) 1st step	115	21.68	0.833	$A_{3/2}$; $n = 1.5$, $m = 0.5$	102; 103	19.24; 20.53
PLAC/PTMC (air) 2nd step	143	25.61	0.207	$A_{3/2}$; $n = 1.5$, $m = 0.5$	135; 143	24.33; 26.83

[a] Constant rate calculated using the Arrhenius equation ($k = A_{inv}\exp(-E_{inv}/RT)$) and at temperatures of 360°C.

All methods gave an almost similar activation energy, as summarized in Table IV, which ranges between 111 and 120 kJ/mol and agrees with the 119 kJ/mol obtained from the isothermal analysis.

The Coats–Redfern method was chosen to determine the thermal degradation mechanism. According to eq. (6), the activation energy for every $g(\alpha)$ function listed in Table I was calculated at constant heating rates by fitting a linear plot of ln $g(\alpha)/T^2$ versus $1/T$. The slope of this representation allows the activation energy to be determined for each possible model and the model to be selected by considering the agreement with the previously calculated activation energy (Table IV). If two or more models are selected, the one having the best regression coefficient is chosen. Note that, with this methodology it is possible to know the complete kinetic triplet (E, A, and $g(\alpha)$) if the intercept at the origin of the linear plot is also considered.

To find the influence of the heating rate, we applied the Coats–Redfern methodology to the five heating rates considered (for conversions between 0.1 and 0.9). Data summarized in Tables V and VI showed almost similar E values for all heating rates, although those obtained at 3°C/min were in slightly better agreement with the values deduced by the Kissinger, Friedman, and Ozawa methods. Works performed with poly(dodecamethylene-isophthalamide)[34] and poly(*p*-dioxanone)[19] indicated that the best agreement was also achieved at lowest heating rates.

Analysis of the results obtained by the Coats–Redfern method showed that the degradation mechanism under both N_2 and air follows a sigmoidal ($A_{3/2}$) mechanism since the activation energies compare well with those obtained with isoconversional methods and good regression coefficients are obtained. To corroborate the kinetic model, the IKP method was also used, the invariant parameters being summarized in Table VII.

Note that although the activation energies for isothermal and nonisothermal degradations are similar, there are significant differences between the preexponential factors. The most striking difference between both kinds of degradation is that the reaction mechanisms (F_1 for isothermal and $A_{3/2}$ for nonisothermal) involved are not the same. To verify this assertion, we simulated the isothermal experimental data using the isoconversional data from the nonisothermal analysis. Hence, conversion and time for a given isothermal temperature were related using the equation

$$\ln t = \ln[g(\alpha)/A] + E/RT \tag{20}$$

The linear representations of ln (β/T^2) versus $1/T$ allow the kinetic parameter ln[$AR/g(\alpha)E$] to be determined for every value of α. This constant is directly related by R/E to the constant ln[$g(\alpha)/A$] of the isothermal adjustment.

Figure 8 shows a clear disagreement between experimental and simulated curves at the higher assayed isothermal temperatures. This demonstrates that isothermal and nonisothermal processes follow a different mechanism, although a relative good agreement is observed at lower temperatures when degradation takes place at a lower rate (e.g. 260°C).

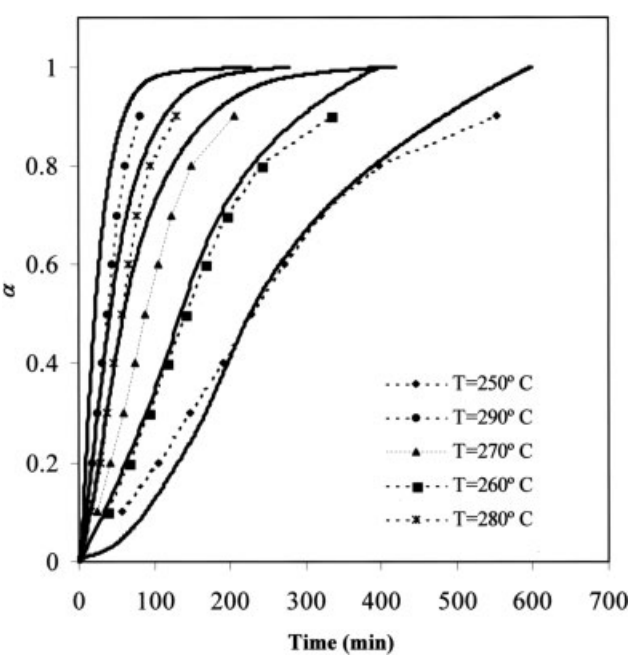

Figure 8 Experimental (continuous lines) and simulated (dotted lines) isothermal curves for the PLAC/PTMC degradation.

TABLE VIII
Thermogravimetric Data of PLAC/PTMC Samples

β (°C/min)	$T_{20\%}$ (°C)	$T_{50\%}$ (°C)	$T_{70\%}$ (°C)	$T_{90\%}$ (°C)	T_{max} (°C)	
1.5	267.81	295.41	317.61	339.01	280.29	324.6
3	283.05	306.08	329.62	350.56	300.35	339.53
5	297.23	318.87	336.78	356.63	314.11	343.92
7	303.33	323.29	335.52	359.45	322.57	353.00
10	311.35	331.57	341.96	365.72	332.72	362.04
20	332.21	351.31	360.63	373.11	357.63	
25	343.43	360.01	369.23	38.,4	361.27	
30	344.78	365.85	374.57	385.97	370.91	
40	359.71	379.47	389.04	401.07	383.59	

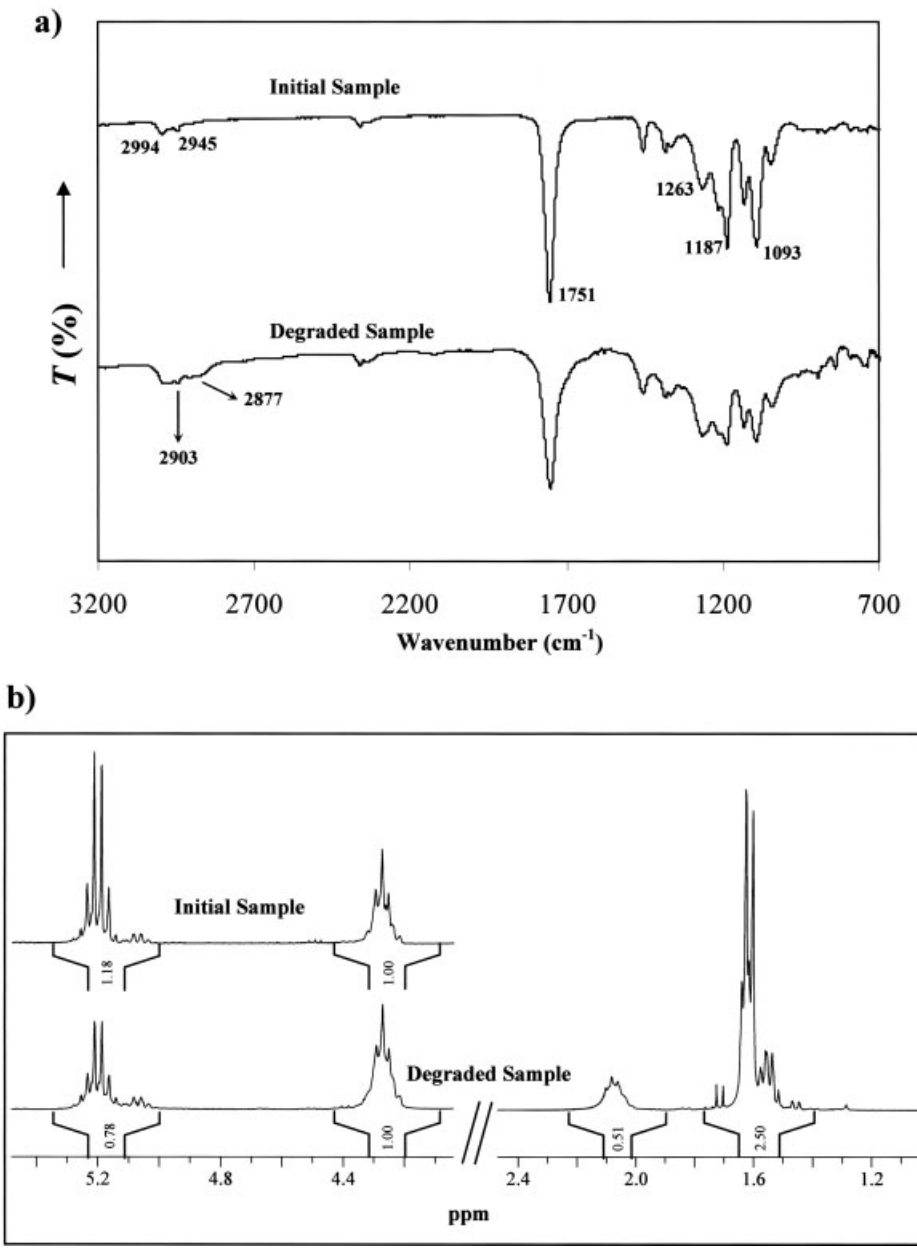

Figure 9 Infrared (a) and ^{1}H-NMR spectra (b) of the initial PLAC/PTMC sample and after a weight loss of 45% in a dynamic thermal decomposition experiment performed at 1.5°C/min.

Kinetics of nonisothermal thermal degradation of PLAC/PTMC

Thermogravimetric data of PLAC/PTMC decomposition under air at five heating rates varying from 1.5 to 40°C/min are summarized in Table VIII, whereas representative curves of low and high heating rates are plotted in Figure 6. Curves obtained at low rates (from 1.5 to 10°C/min) show two steps, which suggest the existence of two different degradation mechanisms. Distinction becomes increasingly difficult when the heating rate is increased and only one step can be distinguished at rates equal or greater than 20°C/min. The first step corresponds to the highest mass loss (around 60%) and may be mainly attributed to a decomposition that involves the lactide units.

The infrared spectrum of the residue obtained at the end of the first step (45% weight loss) by heating the sample at 1.5°C/min showed the characteristic absorption bands of the initial sample [Fig. 9(a)]. The main changes correspond to the 3000–2850 cm^{-1} zone, where CH_2 bands (2903 and 2877 cm^{-1}) indicated an increase in trimethylene carbonate content. ^{1}H-NMR spectra show the characteristic signals of the polymer again, although the ratio between lactidyl and trimethylene carbonate units changes [Fig. 9(b)]. Thus, the lactidyl molar content decreases to 61% (from an initial value of 70%), indicating that a preferential lactide ring formation occurs during this first degradation step. However, it should also be pointed out that trimethylene carbonate units must be also produced during decomposition since a lactidyl content close to 31% is calculated when it is assumed that the 45% weight loss concerns lactidyl units only.

The existence of various overlapping degradation processes complicated the nonisothermal determination of the complete kinetic triplets associated with each degradation process. To solve this problem, a mathematical deconvolution of the derivated thermogravimetric analysis (DTGA) curves was carried out for the experiments performed at low heating rates.

Figure 10 shows the characteristic plots corresponding to the FWO and Friedman analyses of PLAC/PTMC samples. The activation energies are summarized in Table IV, whereas isoconversional data obtained from the FWO and Friedman methods are summarized in Table IX. All procedures gave similar activation energy for the first step (83–119 kJ/mol), which was comparable with that determined for the PLAC/PTMC copolymer and lower than the value obtained for the second degradation step (139–162 kJ/mol).

Analysis of the results obtained by the Coats–Redfern methodology (Table X) showed that both the sigmoidal $A_{3/2}$ and the autocatalytic ($n = 1.5$; $m = 0.5$) mechanisms were possible for each degradation step of PLAC/PTMC. To choose the appropriate mechanism, the invariant parameters (Table VII) were calculated by using the IKP method again. A slightly better fit was found for the second step considering the autocatalytic process. However, it should be noted

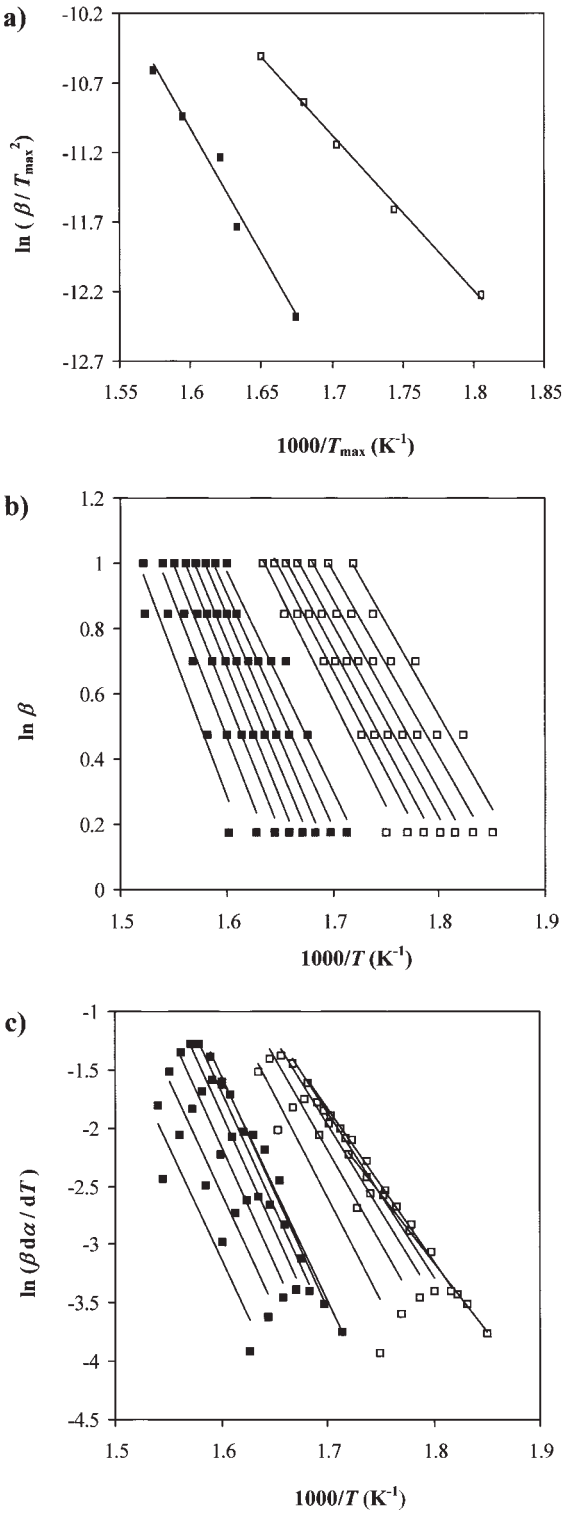

Figure 10 Kissinger (a), FWO (b), and Friedman (c) plots for the thermal decomposition of the PLAC/PTMC sample in air. The first and the second degradation steps are indicated by empty and full symbols, respectively.

TABLE IX
Activation Energies of PLAC/PTMC in Air Atmosphere Obtained by Flynn–Wall–Ozawa and Friedman Methods

Conversion	Flynn-Wall-Ozawa method						Friedman method					
	Single step[a]		Step 1[b]		Step 2[b]		Single step[i]		Step 1[b]		Step 2[b]	
α	*E* (kJ/mol)	*r*	*E* (kJ/mol)	*r*	*E* (kJ/mol)	*r*	*E* (kJ/mol)	*r*	*E* (kJ/mol)	*r*	*E* (kJ/mol)	*r*
0.1	71	0.9461	103	0.9598	111	0.9741	89	0.9695	94	0.9980	151	0.9946
0.2	77	0.9785	104	0.9832	123	0.9808	83	0.9795	97	0.9999	160	0.9933
0.3	80	0.9946	104	0.9904	131	0.9846	84	0.9713	102	0.9997	164	0.9923
0.4	80	0.9977	106	0.9938	138	0.9854	83	0.9934	109	0.9978	166	0.9892
0.5	79	0.9974	107	0.9938	142	0.9835	82	0.9949	116	0.9919	165	0.9809
0.6	80	0.9976	110	0.9920	146	0.9835	83	0.9831	124	0.9778	165	0.9722
0.7	81	0.9949	114	0.9889	150	0.9795	91	0.9752	132	0.9542	163	0.9534
0.8	82	0.9942	118	0.9793	152	0.9691	96	0.9917	145	0.9127	160	0.9182
0.9	85	0.9947	122	0.9491	157	0.9536	99	0.9795	148	0.8294	164	0.9011
Mean	79		110		139		88		119		162	

[a] Parameters obtained at high heating rates (40–20°C/min).
[b] Parameters obtained at low heating rates (10–1.5°C/min).

that sigmoidal mechanisms are more usual in polymer degradation. Thus, the $A_{3/2}$ model could be selected for the first step in agreement with that found for the PGL/PTMC degradation.

When the analyses were performed at higher heating rates (single degradation step), a sigmoidal mechanism (A_2 model) was found (Table XI). However, it should be noted that in this case the deduced kinetic parameters (Table VII) have no physical sense since two mechanisms are actually involved.

To compare the thermal stability of the two processes for PLAC/PTMC and between this and PLG/PTMC, the activation energy value should not be used exclusively due to the compensating effect present between *E* and *A*. Thus, kinetic constant values are also indicated in Table VII for comparison purposes. These constants were calculated using the Arrhenius equation at a representative temperature (360°C) and using the invariant parameters. Note that the kinetic model ($f(\alpha)$) is not considered in the equation, and consequently, precautions should be taken when reactions with a different mechanism are compared. The kinetic rate constant of PGL/PTMC (0.286 min^{-1}) was lower than that of the first step for PLAC/PTMC (0.833 min^{-1}). This great difference indicates a faster degradation rate for the lactide derivative, since in addition, the degradation mechanism is similar. The second step has a clearly lower kinetic constant (0.267 min^{-1}), which is of the same magnitude order as that found for PTMC. Finally, note that the kinetic constant calculated for PLAC/PTMC by using the high heating rate data has an intermediate value (0.507 min^{-1}) between those determined for the two degradation steps.

TABLE X
Activation Energies of PLAC/PTMC in Air Atmosphere Obtained by Coats–Redfern Method

Model	20°C/min		25°C/min		30°C/min		40°C/min	
	E (kJ/mol)	*R*	*E* (kJ/mol)	*R*	*E* (kJ/mol)	*R*	*E* (kJ/mol)	*R*
Power	58	0.9920	66	0.9850	55	0.9977	61	0.9932
$A_{3/2}$	113	0.9995	131	0.9996	108	0.9953	120	0.9995
A_2	82	0.9995	96	0.9995	78	0.9950	87	0.9995
A_3	52	0.9994	60	0.9995	49	0.9944	55	0.9995
A_4	36	0.9993	43	0.9994	34	0.9936	38	0.9994
F_1	175	0.9995	202	0.9996	167	0.9956	186	0.9995
R_2	148	0.9985	170	0.9956	142	0.9988	157	0.9991
R_3	157	0.9993	180	0.9974	150	0.9981	166	0.9998
D_1	261	0.9939	296	0.9882	252	0.9982	276	0.9948
D_2	299	0.9974	339	0.9937	288	0.9991	316	0.9981
D_3	324	0.9994	370	0.9976	310	0.9982	342	0.9998
D_4	300	0.9982	342	0.9950	288	0.9990	318	0.9988
$n = 1.5$	207	0.9965	240	0.9993	196	0.9888	219	0.9958
$n = 1.5$, $m = 0.5$	116	0.9899	136	0.9953	109	0.9780	124	0.9883
$n = 1.9$, $m = 0.1$	218	0.9906	253	0.9956	205	0.9795	231	0.9891
$n = 2$	243	0.9907	283	0.9956	229	0.9797	258	0.9892
$n = 3$	326	0.9757	383	0.9840	305	0.9599	347	0.9728

TABLE XI
Activation Energies of PLAC/PTMC in Air Atmosphere Obtained by Coats–Redfern Method at 3°C/min

	Step 1		Step 2	
	E (kJ/mol)	r	E (kJ/mol)	r
Power	52	0.9972	68	0.9760
$A_{3/2}$	102	0.9978	135	0.9974
A_2	74	0.9977	99	0.9973
A_3	46	0.9975	63	0.9969
A_4	32	0.9972	44	0.9965
F_1	157	0.9980	208	0.9976
R_2	134	0.9999	174	0.9907
R_3	141	0.9997	185	0.9935
D_1	238	0.9979	301	0.9806
D_2	271	0.9995	345	0.9882
D_3	292	0.9997	379	0.9938
D_4	272	0.9998	350	0.9899
$n = 1.5$	184	0.9923	249	0.9999
$n = 1.5$, $m = 0.5$	103	0.9928	143	0.9986
$n = 1.9$, $m = 0.1$	193	0.9839	265	0.9987
$n = 2$	215	0.9841	295	0.9987
$n = 3$	286	0.9652	404	0.9908

CONCLUSIONS

The kinetics of thermal degradation of PGL/PTMC (Maxon) has been studied in isothermal and nonisothermal conditions. The isothermal degradation under air follows a first order mechanism with an activation energy of 119 kJ/mol and a preexponential factor of 4.24×10^9 min^{-1}. A change in the degradation mechanism is observed in the nonisothermal experiments. Thus, a sigmoidal $A_{3/2}$ model with an activation energy of 115–117 kJ/mol and a preexponential factor of $0.8–1.3 \times 10^9$ min^{-1} is determined in the degradations performed under nitrogen and air. We have observed that the degradation behavior under a nitrogen atmosphere is similar from that under air.

Semicrystalline copolymers with a blocky distribution of lactyl units, and a similar molar content of trimethylene carbonate units to that of the studied PGL/PTMC copolymer can be obtained by ring opening polymerization of lactide and trimethylene carbonate monomers, conducted at 150°C and using $Sn(Oct)_2$ as a catalyst.

Two clear steps of decomposition have been observed for the nonisothermal degradation of PLAC/PTMC under air, in contrast with the single step observed for the glycolide copolymer. The first step corresponds to a preferential depolymerization of the lactidyl units and involves a sigmoidal $A_{3/2}$ model with an activation energy close to 115 kJ/mol and a preexponential factor of 2.6×10^9 min^{-1}. The second step has an activation energy close to 143 kJ/mol and a preexponential factor of 8.0×10^{10} min^{-1}. Heating rates for nonisothermal analyses have to be accurately selected to distinguish the different steps involved in the thermal degradation of PLAC/PTMC.

Degradation studies performed with copolymers constituted by a similar ratio between trimethylene carbonate and lactidyl or glycolyl units demonstrate a lower thermal stability for the lactidyl derivative. In spite of this, kinetic studies demonstrate that in both cases the degradation rate is low at temperatures slightly higher than the melting ones, so processing from the melt can be carried out without a significant molecular weight loss.

References

1. Chu, C. C. Wound Closure Materials and Devices; CRC Press: Boca Raton, Florida, 1997; pp 65–106.
2. Domb, A. J.; Kost, J.; Wiseman, D. M. Handbook of Biodegradable Polymers; Harwood Academic Publishers: Amsterdam, 1997.
3. Schmitt, E. E.; Polistina, R. A. U.S. Pat. 3,297,033 (1967).
4. Schneider, A. K. U.S. Pat. 2,703,316 (1955).
5. Ray, J. A.; Doddi, N.; Regula, D.; Williams, J. A.; Melverger, A. Surg Gynecol Obstet 1981, 153, 497.
6. Rosensaft, P. L.; Webb, R. L. U.S. Pat. 4,243,775 (1981).
7. Bezwada, R. S.; Jamiolkowski, D. D.; Lee, I. Y.; Agarwal, V.; Persivale, J.; Trenka-Bethin, S.; Erneta, M.; Persivale, J.; Suryadevara, J.; Yang, A.; Liu, S. Biomaterials 1995, 16, 1141.
8. Katz, A. R.; Mukherjee, D. P.; Kagonov, A. L.; Gordon, S. A. Surg Gynecol Obstet 1985, 161, 213.
9. Pospiech, D.; Komber, H.; Jehnichen, D.; Hausler, L.; Eckstein, K.; Scheibner, H.; Janke, A.; Kricheldorf, H. R.; Petermann, O. Biomacromolecules 2005, 6, 439.
10. Metz, S. A.; Chegini, N.; Masterson, B. J Biomater 1990, 11, 41.
11. Lee, K. L.; Chu, C. C. J Biomed Mater Res 1999, 49, 25.
12. Dobrzynski, P.; Kasperczyk, J. J Polym Sci, Part A: Polym Chem 2006, 44, 98.
13. Hill, S. P.; Montes de Oca, H.; Klein, P. G.; Ward, I. M.; Rose, J.; Farrar, D. Biomaterials 2006, 27, 3168.
14. Zurita, R.; Puiggalí, J.; Franco, L.; Rodríguez-Galán, A. J Polym Sci, Part A: Polym Chem 2006, 44, 993.
15. Cooper, D. R.; Sutton, G. J.; Tighe, B. J. J Polym Sci, Part A: Polym Chem 1973, 11, 2045.
16. McNeill, I. C.; Leiper, H. A. Polym Degrad Stab 1985, 11, 309.
17. Kopinke, F. D.; Remmler, M.; Mackenzie, K.; Möder, M.; Wachsen, O. Polym Degrad Stab 1996, 53, 329.
18. Nishida, H.; Yamashita, M.; Hattori, N.; Endo, T.; Tokiwa, Y. Polym Degrad Stab 2000, 70, 485.
19. Yang, K. K.; Wang, X. L.; Wang, Y. Z.; Wu, B.; Jin, Y. D.; Yang, B. Eur Polym J 2003, 39, 1567.
20. Vyazovkin, S.; Dollimore, D. J Chem Inform Comput Sci 1996, 36, 42.
21. Coats, A.; Redfern, J. P. Nature 1964, 201, 68.
22. Kissinger, H. E. Anal Chem 1957, 29, 1702.
23. Friedman, H. J Polym Sci C 1964, 6, 183.
24. Ozawa, T. Bull Chem Soc Jpn 1965, 38, 1881.
25. Flynn, J. H.; Wall, L. A. J Res Natl Bur Stand, Part A: Phys Chem 1966, 70, 487.
26. Mianowskin, A. J Therm Anal Calorim 2003, 74, 953.
27. Lesnikovich, A. I.; Levchik, S. V. J Therm Anal 1983, 27, 89.
28. Lesnikovich, A. I.; Levchik, S. V. J Therm Anal 1985, 30, 677.
29. Draney, D. R.; Jarrett, P. K. Polym Prepr (Am Chem Soc, Div Polym Chem) 1990, 31, 137.
30. Flory, P. J Trans Faraday Soc 1955, 51, 848.
31. Fischer, E. W.; Sterzel, H. J.; Wegner, G. Kolloid Z Z Polym 1973, 251, 980.
32. Vasanthakumar, R.; Pennings, A. J. Polymer 1983, 24, 175.
33. Tsuji, H.; Ikada, Y. Polymer 1995, 36, 2709.
34. Minying, L.; Lijun, G.; Qingxiang, Z.; Yudong, W.; Xiaojuan, Y.; Shaokui, C. Chem J Internet 2003, 5, 43.